



This is the accepted manuscript made available via CHORUS. The article has been published as:

## Magnon-polaron driven thermal Hall effect in a Heisenberg-Kitaev antiferromagnet

N. Li, R. R. Neumann, S. K. Guang, Q. Huang, J. Liu, K. Xia, X. Y. Yue, Y. Sun, Y. Y. Wang, Q. J. Li, Y. Jiang, J. Fang, Z. Jiang, X. Zhao, A. Mook, J. Henk, I. Mertig, H. D. Zhou, and X. F. Sun

Phys. Rev. B **108**, L140402 — Published 4 October 2023

DOI: [10.1103/PhysRevB.108.L140402](https://doi.org/10.1103/PhysRevB.108.L140402)

# Magnon-Polaron Driven Thermal Hall Effect in a Heisenberg-Kitaev Antiferromagnet

N. Li,<sup>1,\*</sup> R. R. Neumann,<sup>2,\*</sup> S. K. Guang,<sup>1,\*</sup> Q. Huang,<sup>3</sup> J. Liu,<sup>3</sup> K. Xia,<sup>1</sup> X. Y. Yue,<sup>4</sup> Y. Sun,<sup>4</sup>  
Y. Y. Wang,<sup>4</sup> Q. J. Li,<sup>5</sup> Y. Jiang,<sup>5</sup> J. Fang,<sup>6</sup> Z. Jiang,<sup>6</sup> X. Zhao,<sup>7</sup> A. Mook,<sup>8</sup> J. Henk,<sup>2</sup>  
I. Mertig,<sup>2,†</sup> H. D. Zhou,<sup>3,†</sup> and X. F. Sun<sup>4,1,†</sup>

<sup>1</sup> Department of Physics, Hefei National Laboratory for Physical Sciences at Microscale, and Key Laboratory of Strongly-Coupled Quantum Matter Physics (CAS), University of Science and Technology of China, Hefei, Anhui 230026, People's Republic of China

<sup>2</sup> Institute of Physics, Martin Luther University Halle-Wittenberg, Halle (Saale), Germany

<sup>3</sup> Department of Physics and Astronomy, University of Tennessee, Knoxville, Tennessee 37996-1200, USA

<sup>4</sup> Institute of Physical Science and Information Technology, Anhui University, Hefei, Anhui 230601, People's Republic of China

<sup>5</sup> School of Physics and Optoelectronics, Anhui University, Hefei, Anhui 230601, People's Republic of China

<sup>6</sup> School of Physics, Georgia Institute of Technology, Atlanta, GA 30332, USA

<sup>7</sup> School of Physical Sciences, University of Science and Technology of China, Hefei, Anhui 230026, People's Republic of China

<sup>8</sup> Institute of Physics, Johannes Gutenberg University, Mainz, Germany

\* These authors contributed equally: N. Li, R. R. Neumann, S. K. Guang.

† Email: ingrid.mertig@physik.uni-halle.de; hzhou10@utk.edu; xfsun@ahu.edu.cn

**We investigate the thermal Hall effect in the Heisenberg-Kitaev antiferromagnet  $\text{Na}_2\text{Co}_2\text{TeO}_6$ , where we observe a negative thermal Hall conductivity (THC) with thermal Hall angles up to 2 % at low magnetic fields, which changes sign to positive THC at higher fields. Our theoretical calculations, incorporating spin-lattice coupling, reveal that the quantum-geometric Berry curvature of magnon polarons counteracts the purely magnonic contribution, resulting in a reversed sign and increased magnitude of the THC. This finding emphasizes the significance of spin-lattice coupling in understanding the thermal Hall effect.**

Topological phases of matter have received enormous attention in solid state physics not only for their exceptional fundamental properties, but also for their potential technological impact. For example, topological band insulators feature protected, dissipationless edge

channels [1–3], and topological order in strongly correlated electron systems (e.g., quantum spin liquids [4–6]) may be a route to fault-tolerant quantum computing. [7,8] Harvesting the potential of these exotic phases requires a reliable technique for their detection and characterization. An important probe for topological phases in insulators is the thermal Hall effect (THE), which denotes a transverse heat current response to a longitudinal temperature gradient. [9,10] Its *intrinsic* contribution is an invaluable probe of the Berry curvature, that is, a quantum-geometric property acting on the inherent quasiparticles, e.g., Majorana fermions [11,12], triplons [13,14], photons [15,16], and magnons [17–23], like a fictitious magnetic field. However, the ubiquitous phonons (quanta of lattice vibrations) interact and potentially hybridize with the aforementioned quasiparticles due to spin-lattice coupling (SLC). [24–26] The band inversions of these quasiparticle-phonon hybrids establish another source of Berry curvature that may even dominate the low-temperature THE because of the low acoustic phonon energies. Hence, detailed understanding of SLC and its effects on intrinsic heat transport is required.

In this joint experimental and theoretical work, we report the thermal Hall conductivity (THC)  $\kappa_{xy}$  of the Kitaev spin-liquid candidate  $\text{Na}_2\text{Co}_2\text{TeO}_6$  (NCTO), which has attracted considerable attention recently. [27–42] Our field- and temperature-dependent measurements reveal a negative THC for out-of-plane magnetic fields below 10 T and a positive THC above 10 T at low temperatures. We attribute this sign change to a field-driven magnetic phase transition. As we demonstrate theoretically, magnons fail to explain not only the overall sign of the THC, but also its order of magnitude, as the THC is underestimated by a factor of 10. By taking SLC into account, magnons and phonons form hybrid quasiparticles, i.e., magnon polarons. The Berry curvature at the resulting avoided crossing between the lowest magnon and the acoustic phonon band is of opposite sign compared to the low-energy magnon Berry curvature without SLC. Hence, we reproduce both the correct overall sign and the order of magnitude of the experimental THC. The sign reversal of the THC due to the hybridization of phonons and magnons is one of our main findings that is visualized in Figure 1. Our results indicate the pivotal role of the SLC in thermal transport, which may be also relevant to the interpretation of the THC in related Heisenberg-Kitaev magnets. [43–45]

NCTO is composed of  $\text{Co}^{2+}$  ions, arranged in layers of honeycomb lattices, whose effective  $S = \frac{1}{2}$  spins order in antiferromagnetic (AFM) zigzag chains (cf. Figure 2a). Employing a three-thermometer setup (panel b; cf. Supplemental Material (SM) [46]), we have measured the temperature dependence of the longitudinal thermal conductivity  $\kappa_{xx}(T)$  of NCTO at zero magnetic field (panel c). According to previous studies, NCTO enters a

magnetically ordered state below the Néel temperature  $T_N = 27$  K, followed by two possible spin reorientations around 16 K and 6 K, respectively. [27–31] Our  $\kappa_{xx}(T)$  data show no obvious anomalies around 27 K and 16 K, in agreement with reported  $\kappa_{xx}(T)$  data, [47] but a slope change below around 6 K possibly related to a spin reorientation. [28,30] At sub-Kelvin temperatures,  $\kappa_{xx}(T)$  roughly follows a  $T^{1.2}$  behavior, which is at variance with the  $T^3$  or  $T^2$  behavior expected for the phonon thermal conductivity at low temperatures in 3 or 2 dimensions, respectively. [48] Since magnons are frozen out at temperatures corresponding to energies below the spin-wave gap, their contribution does not explain the observed scaling law either. Therefore, this  $T^{1.2}$  behavior may indicate the significance of interactions between phonons and magnons.

The field dependence of  $\kappa_{xx}(B)$  measured at various temperatures with  $\mathbf{B} \parallel \mathbf{c}$  is depicted in Figures 2d and 2e. At  $T < 1.56$  K,  $\kappa_{xx}(B)$  decreases quickly with increasing field to reach a minimum around 4 T, and then shows a weak field dependence up to 14 T. At 2.2 K, 2.7 K, and 3.2 K,  $\kappa_{xx}(B)$  manifests a double-valley structure with valleys around 2 T and 10 T, respectively. At even higher temperatures,  $\kappa_{xx}(B)$  exhibits a broad valley in the range of 5 – 10 T. Similar observations have been reported in Ref. [49].

Apart from the complex longitudinal thermal conductivity, we find a peculiar field dependence of the THC  $\kappa_{xy}(B)$ , which we have measured at various temperatures below  $T_N$  (cf. Figures 3a,b). At  $T \leq 2.2$  K, with increasing field,  $\kappa_{xy}(B)$  first exhibits a negative Hall response reaching a minimum around 3 to 5 T; then it changes to positive sign around 10 T and increases at higher fields. At 3.2 K and 5.4 K,  $\kappa_{xy}(B)$  curves show a positive peak at low fields, followed by two zero crossings with increasing field. At 7.8 K,  $\kappa_{xy}(B)$  is positive without sign reversal. We have plotted the temperature dependence of  $\kappa_{xy}/T$  at several fields in Figure 3c. It is evident that at  $B = 3$  T and 5 T, with increasing temperature,  $\kappa_{xy}$  is negative and reaches a minimum around 2 K, and then changes to positive sign around 3 K to 4 K. The thermal Hall angle  $\kappa_{xy}/\kappa_{xx}$  possesses a minimum around 4 T and changes to positive sign around 10 T at temperatures below 2.2 K (cf. Figure 3d). The largest absolute value of  $\kappa_{xy}/\kappa_{xx}$  is around 2 % at 0.78 K and 4 T.

In a magnetic insulator, the observed  $\kappa_{xy}$  may have several origins, including phonons, magnons, and fractionalized exotic quasiparticles such as spinons. In experiments on nonmagnetic insulators,  $\kappa_{xy}$  of phonons does not exhibit a sign change, [49,50] although this possibility cannot be ruled out here. For spinons, a nonzero  $\kappa_{xy}$  has only been observed in a quantum spin liquid with disordered spins. [51–53] Apparently, these two scenarios cannot

explain the sign-reversible and non-monotonic  $\kappa_{xy}(B)$  observed in the AFM state of NCTO. Moreover, the 2 % thermal Hall angle is exceptionally large for an insulator. The expected value, either originating from phonons or magnons, is typically around 0.3 % to 0.6 % or even lower, [54] although similar thermal Hall angles have been observed in the insulating phases of the cuprate  $\text{Nd}_{2-x}\text{Ce}_x\text{CuO}_4$  (up to 2 %), [55] the iridate  $\text{Sr}_2\text{Ir}_{1-x}\text{Rh}_x\text{O}_4$  (up to 3 %), [56] and the pyrochlore magnet  $\text{Yb}_2\text{Ti}_2\text{O}_7$  in its quantum spin-liquid state (up to 2 %). [53]

The experimental results on the transverse transport properties of NCTO are subsequently explained by an effective, semi-quantitative model. The starting point is the Heisenberg-Kitaev-Gamma-Gamma' (HKGG') Hamiltonian [57–59]

$$H = \frac{1}{2\hbar^2} \sum_{\langle ij \rangle_r} J_r \mathbf{S}_i \cdot \mathbf{S}_j + \frac{1}{2\hbar^2} \sum_{\langle ij \rangle} \left[ K S_i^\gamma S_j^\gamma + \Gamma (S_i^\alpha S_j^\beta + S_i^\beta S_j^\alpha) + \Gamma' (S_i^\gamma S_j^\alpha + S_i^\alpha S_j^\gamma + S_i^\beta S_j^\beta + S_i^\beta S_j^\beta) \right]$$

that encompasses Heisenberg exchange [ $J_r$  ( $r = 1, 2, 3$ )] up to 3<sup>rd</sup> nearest neighbors and Kitaev ( $K$ ), Gamma ( $\Gamma$ ), Gamma' ( $\Gamma'$ ) interactions between nearest neighbors. The magnetic field  $\mathbf{B}$  enters via the Zeeman Hamiltonian

$$H_B = \frac{g\mu_B}{\hbar} \mathbf{B} \cdot \sum_i \mathbf{S}_i.$$

Here, we are interested in out-of-plane fields  $\mathbf{B} \parallel \mathbf{c}$ . Several parameter sets of the spin Hamiltonian have been determined for NCTO. [46] In the following, we choose  $J_1 = -3.2$  meV,  $J_2 = 0.1$  meV,  $J_3 = 1.2$  meV,  $K = 2.7$  meV,  $\Gamma = -2.9$  meV, and  $\Gamma' = 1.6$  meV. [36] This parameter set (referred to as tc+) reproduces the critical fields in experimental reports on field-induced magnetic phase transitions [46] and, as presented below, provides the best agreement with the experimental THC. Results for other parameter sets are reported in the SM. [46] The weak inter-layer coupling is neglected.

The antiferromagnetic ground state of the Hamiltonian at zero field is characterized by zigzag chains with intra-chain ferromagnetic and inter-chain antiferromagnetic order. Applying a magnetic field cants the spins slightly, but they remain confined to the  $bc$  plane (cf. left inset in Figure 4a). At the critical field of  $B_{c1} = 10.8$  T the system passes a first-order phase transition into a spin-flop state, in which the spins lie within the  $ac$  plane (ferromagnetic component along  $c$  and Néel vector along  $a$ ; cf. right inset in Figure 4a). The magnetization saturates at  $B_{c2} = 31.2$  T, at which the fully field-polarized phase is reached. These critical fields are supported by magnetometry measurements. [46]

The diagonalization of the linearized Hamiltonian yields the four magnon bands  $\varepsilon_{nk}$  ( $n = 1, 2, 3, 4$ ). [60,61] Because of the spin-1/2 nature of the local magnetic moments, significant quantum fluctuations [62,63] are expected, which we discuss in the SM. The

intrinsic contribution to the THC is computed with the linear response formalism (cf. SM). [46,64]

Figure 4a shows  $\kappa_{xy}$  versus  $B_z$  as computed from free-magnon calculations for six temperatures. In the low-field phase,  $\kappa_{xy}$  is positive and changes sign at  $B_{c1}$  for all temperatures. This sign change is thus linked to the magnetic phase transition. However, the overall sign of  $\kappa_{xy}$  is at variance with the measured data (cf. Figure 3a). Attributed to the first-order transition,  $\kappa_{xy}$  is discontinuous at the phase transition, with maximum left and minimum right of  $B_{c1}$ . Moreover, the experimental data are underestimated by a factor of 10. Similar calculations with other parameter sets taken from the literature fail to reproduce the data as well. [46]

The foregoing suggests that magnons by themselves are not sufficient to explain the experimental data. It has been shown before that the hybridization of magnons and phonons can give rise to a thermal Hall effect. [25,26,65–71] We therefore consider out-of-plane oscillating phonons described by

$$H_p = \sum_i \frac{(p_i^z)^2}{2M} + \frac{C}{4} \sum_{\langle ij \rangle} (u_i^z - u_j^z)^2$$

( $p_i^z$  momentum,  $u_i^z$  displacement), which are subject of a particular SLC arising from spin-orbit coupling: [25,26,67,71–73]

$$H_{me} = \frac{\tilde{\lambda}}{\hbar^2} \sum_i \sum_{\delta} (\mathbf{S}_i \cdot \boldsymbol{\delta}) S_i^z (u_i^z - u_{i+\delta}^z)$$

( $\boldsymbol{\delta}$  nearest neighbor bond vectors for site  $i$ ). We neglect vibrations of nonmagnetic ions and other types of SLC for a minimal description. Furthermore, we consider a single acoustic phonon branch in the crystallographic Brillouin zone (that is, two branches in the magnetic Brillouin zone). The relevant energy scale  $\lambda = \tilde{\lambda} d_{nn} \sqrt{\frac{\hbar}{2\sqrt{CM}}}$  ( $M$  mass of  $\text{Co}^{2+}$ ,  $d_{nn} = 3.0361\text{\AA}$  (in-plane) nearest-neighbor distance) quantifies the strength of the SLC. The elastic constant  $C$  is chosen to yield a phonon velocity of  $3000 \frac{\text{m}}{\text{s}}$ , which is supported by heat capacity measurements. [46,74] We proceed by bosonizing spin and position operators and extend the basis by the two phonon modes. The extended Hamiltonian is then diagonalized, and  $\kappa_{xy}$  is computed as before. The SLC strength  $\lambda = 0.4 \text{ meV}$  has been fitted as an effective parameter to reproduce the experimental THC at 2.2 K.

Figure 4b displays  $\kappa_{xy}$  versus  $B_z$  in the presence of SLC. Compared to exclusive magnon transport, the overall sign of  $\kappa_{xy}$  is reversed and the sign change at the magnetic phase

transition remains intact. Furthermore,  $\kappa_{xy}$ 's order of magnitude has increased and matches that of the experimental data. In short, agreement with the experiment has increased significantly.

The sign change and the increase of  $|\kappa_{xy}|$  are attributed to hybrid quasiparticles that we refer to as magnon polarons. These normal modes are superpositions of magnons and phonons. Their hybrid nature is prominent in the band structure with SLC (Figure 4c) at avoided crossings: their character changes continuously from magnon- (red) to phonon-like (blue). The avoided crossing between the acoustic phonon branch and the lower magnon band generates positive Berry curvature in the lowest band, indicated by a white arrow in panel d. This pronounced low-energy Berry curvature dominates the transport and explains the negative sign in the zigzag antiferromagnetic phase. This finding is contrasted with the Berry curvature in the absence of SLC (panel e). Ignoring the phonon bands (blue in panel c), the magnon bands exhibit a spin-wave gap, and their lowest energies are at the  $\Gamma$  and S points. The Berry curvature of the lowest magnon band (panel e) at these points is negative and positive, respectively. Since the two lower magnon bands are degenerate at S and the upper band exhibits the opposite Berry curvature at S, the Berry curvature at  $\Gamma$  mostly governs the thermal transport at low temperatures. This Berry curvature is, however, opposite to the emerging Berry curvature caused by the hybridization. Thus, there is a competition between pure magnon transport and magnon-polaron transport in the presence of SLC.

The gradual suppression and sign reversal of  $\kappa_{xy}$  by the coupling to phonons hold for lower temperatures. At higher temperatures, the magnon bands are strongly populated and the transport coefficient changes sign back. [46] This competitive interplay between phonons and magnons is contrasted by the results of Zhang *et al.* for the honeycomb ferromagnet  $\text{VI}_3$ , which has been modeled with Dzyaloshinskii-Moriya interaction (DMI) as the source of the magnon Berry curvature. [26] There, an amplification of the THC was found due to the SLC. Notably, an attenuation can be found for reversed DMI, which produces the same magnon spectrum but opposite Berry curvature, and, hence, both amplification and attenuation of the THC are within the reach of the DMI model with SLC. In contrast, the HKGG' model with SLC uniquely fixes both the sign of the magnon and the magnon-polaron Berry curvatures and, therefore, their relative sign. This renders the agreement between theory and experiment nontrivial. Overall, whether the SLC leads to an amplification or an attenuation depends on the spin Hamiltonian and the particular form of the SLC. Examples for the amplification by SLC in the HKGG' model are reported in the SM with different parameters. [46] A systematic study is needed to predict which of these two scenarios can be expected in other systems.

The model including SLC achieves an agreement between theoretical and experimental results in overall sign, magnitude, and the general field dependence, in contrast to the pure magnon calculations. The remaining quantitative disagreement between the effective theoretical model and experiment could be caused by the presence of multiple domains close to the phase transition, which is not accounted for in our model, the restriction to one phonon band and one particular type of SLC, and the disregard of vibrational degrees of freedom of nonmagnetic ions. The deviation between the minima of  $\kappa_{xy}(B_z)$  measured at 3 T and computed at 10 T may be attributed to extrinsic contributions to the THC, as indicated by the correlation between the measured minima of  $\kappa_{xx}$  and  $\kappa_{xy}$  at similar fields (compare Figures 2d,e and 3a). Hence, at lower fields, extrinsic contributions appear to be relevant for a better quantitative agreement, while at larger fields, due to the lack of a similar prominent correlation, their relevance might be limited. Therefore, the extrinsic contributions to the THC such as magnon-phonon scattering, magnon-magnon scattering, and scattering of phonons or magnons at (magnetic) impurities should be investigated in a more comprehensive quantitative theory.

An open question for NCTO is whether its ground state is of zigzag antiferromagnetic or of triple-Q nature. While several studies have argued in favor of triple-Q, [33,39,40] another reports inconsistent observations with the triple-Q ground state. [41] Our study shows that the zigzag antiferromagnetic ground state is compatible with THC measurements, however, we cannot conclusively rule out the possibility of a triple-Q ground state. In the triple-Q state, the noncollinear spin texture gives rise to a more complex SLC and magnon-phonon hybridization leading to a larger set of adjustable parameters, which would have to be obtained from density functional theory. Whether the triple-Q ground state is also compatible with our THC measurements needs to be addressed in the future.

Finally, our results, in particular the fact that magnon polarons and pure magnons can drive opposite heat currents of different magnitudes, demonstrate that the SLC may completely alter the low-temperature transport properties and overshadow predicted transport signatures of isolated quasiparticles, like topological magnons. Instead of transport signatures of isolated exotic spin excitations, a more unified approach that includes the hybridization with phonons is necessary for the interpretation of such transport experiments. To verify the importance of SLC in NCTO, but also more generally, an independent determination of the SLC by ab initio calculations or magnetoelastic experiments is required that should be combined with model calculations to quantify the impact on the THC. In short, our results call for a systematic analysis of the role of SLC in the THC.



## **Acknowledgements**

We thank I. Kimchi for insightful discussions, and W. J. Chu and X. H. Zhou for their help with the experiments. This work was supported by the National Natural Science Foundation of China (Grant Nos. 12274388, 12174361, 12025408, 11904003, and 12274001) and the Nature Science Foundation of Anhui Province (Grant Nos. 1908085MA09, 2108085QA22, and 2208085MA09). The work at the University of Tennessee and Georgia Tech was supported by the U.S. Department of Energy under Award Nos. DE-SC-0020254 and DE-FG02-07ER46451. A. M., J. H., and I. M. acknowledge funding from Deutsche Forschungsgemeinschaft (DFG, German Research Foundation) - Project No. 504261060 and SFB TRR 227.

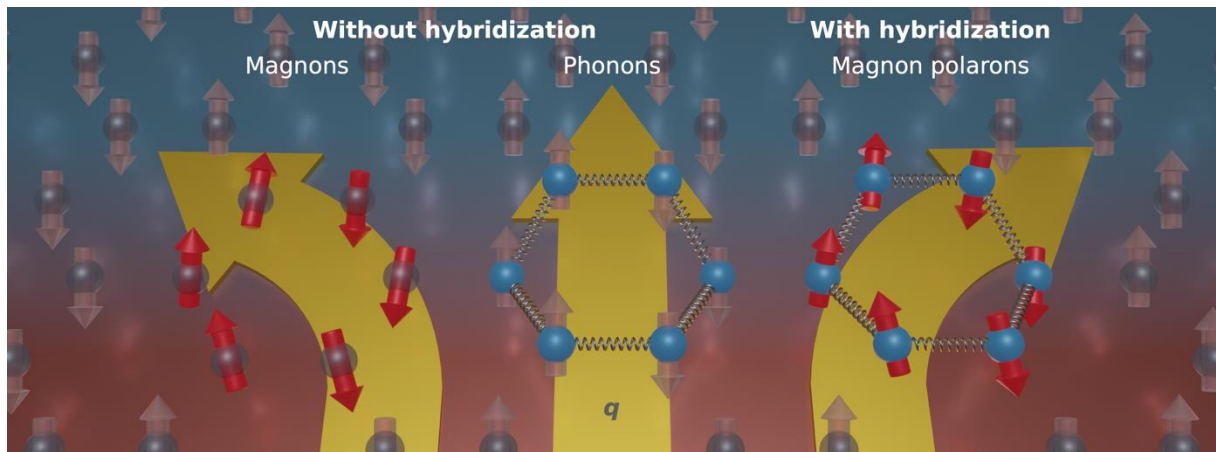


**Figure 1 | Qualitative visualization of our theoretical results.** Intrinsic thermal transport of distinct quasiparticles moving from hot to cold in a temperature gradient. Without hybridization, magnons contribute to the longitudinal and transversal transport, while phonons only contribute to the longitudinal one (in our approximation). With hybridization, magnons and phonons merge into magnon polarons and the transverse transport direction is reversed.

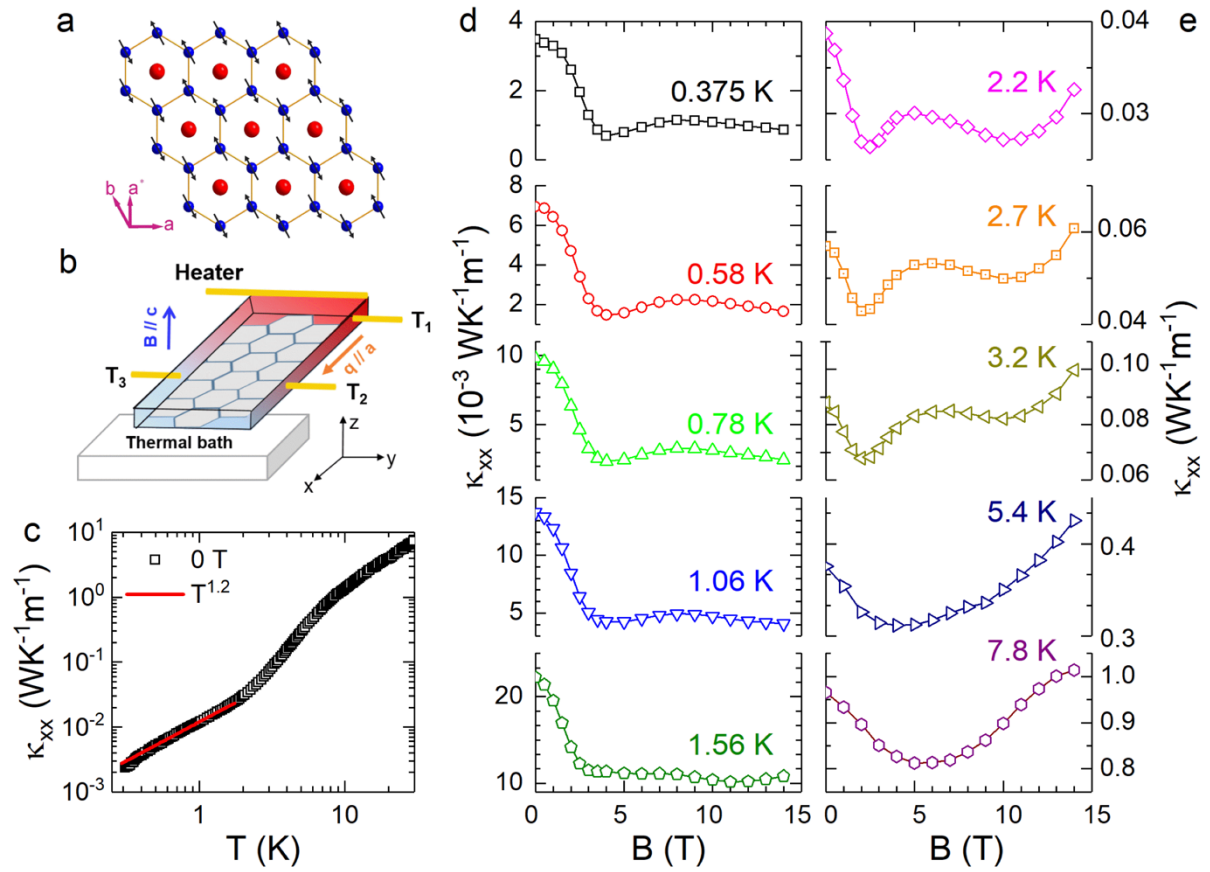


**Figure 2 | Longitudinal thermal heat conductivity  $\kappa_{xx}$  of a  $\text{Na}_2\text{Co}_2\text{TeO}_6$  single crystal. **a**, Crystallographic spin structure of the  $ab$  plane of NCTO in the AFM state. The honeycomb lattice consists of Co ions (blue spheres) in the zigzag AFM arrangements (indicated by arrows), and the Te ions (red spheres) are located at the center of each honeycomb. The  $a^*$  axis is the in-plane direction perpendicular to the  $a$  axis. **b**, Schematic of the experimental setup for the thermal Hall measurements. The heat current and the magnetic field are applied along the  $a$  and  $c$  axis, respectively. The longitudinal and transverse temperature gradients are determined by the difference between  $T_1$  and  $T_2$  and between  $T_2$  and  $T_3$ , respectively. **c**, Temperature dependence of the longitudinal thermal conductivity  $\kappa_{xx}$  at zero magnetic field. The zero-field data roughly display a  $T^{1.2}$  behavior at very low temperatures, as the solid line indicates. **d**, **e**, Magnetic-field dependence of the thermal conductivity at various temperatures and with  $\mathbf{B} \parallel c$ .**

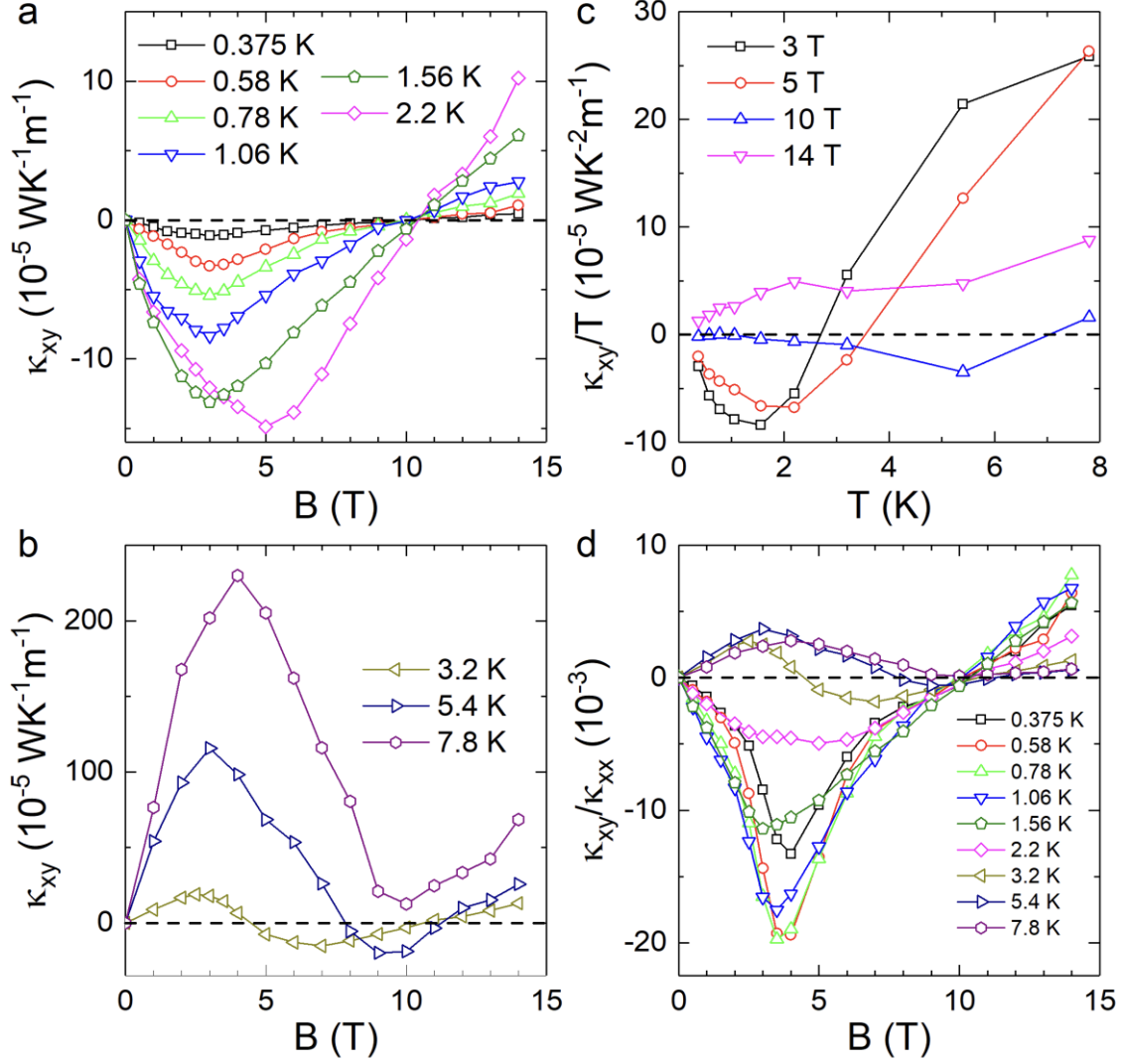


**Figure 3 | Thermal Hall conductivity of a  $\text{Na}_2\text{Co}_2\text{TeO}_6$  single crystal. a, b,** Field dependence of thermal Hall conductivity  $\kappa_{xy}$  for  $B \parallel c$  at various temperatures. **c,** Temperature dependence of  $\kappa_{xy}/T$  at selected magnetic fields. **d,** Magnetic field dependence of the thermal Hall angle  $\kappa_{xy}/\kappa_{xx}$  at various temperatures.

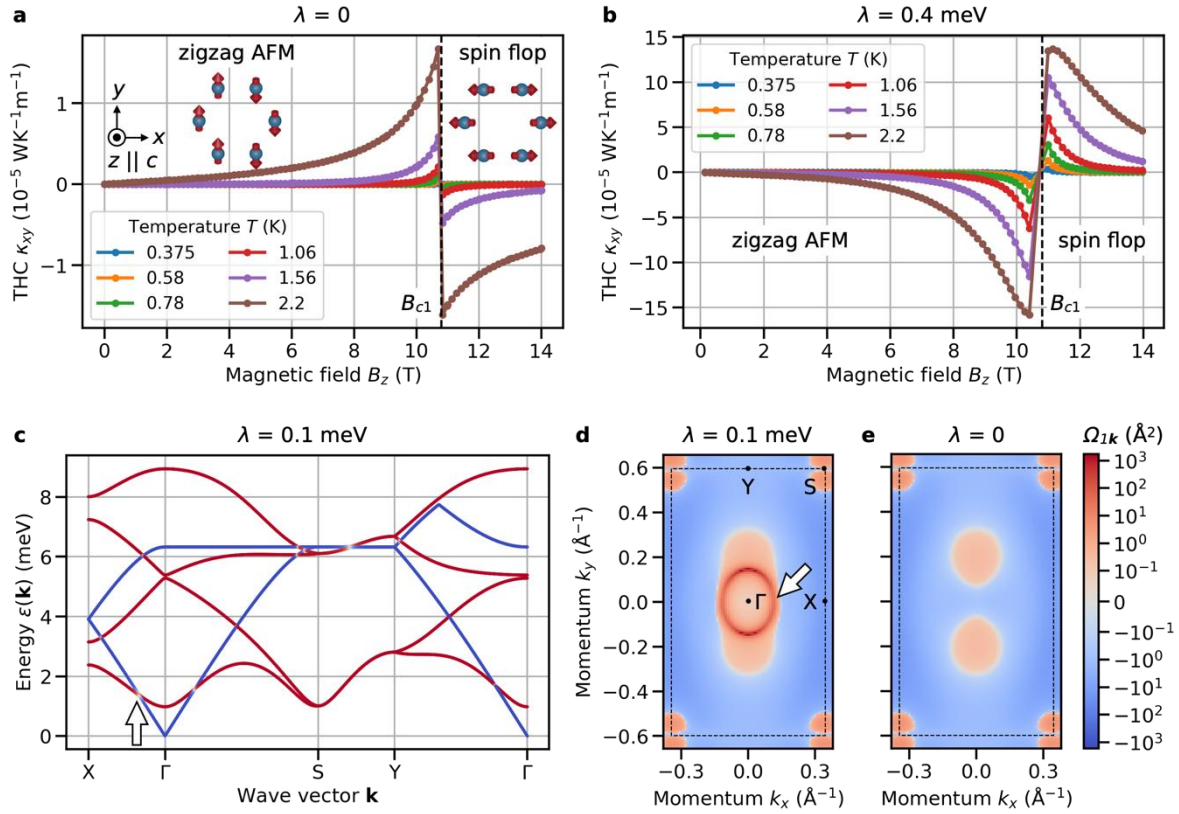


**Figure 4 | Model calculations.** **a, b**, Thermal Hall conductivity  $\kappa_{xy}$  vs applied field  $B_z$  (**a**) without ( $\lambda = 0$  meV) and (**b**) with SLC ( $\lambda = 0.4$  meV). Inset: magnetic ground state of  $\text{Co}^{2+}$  ions in their two respective phases. **c**, Magnon-polaron spectrum  $\varepsilon_{nk}$  along a high-symmetry path. Red/white/blue colored bands indicate magnon/mixed/phonon character of the modes; the magnetic field is 5 T. **d, e**, Berry curvatures  $\Omega_{nk}$  of the lowest bands  $n = 1$  (**d**) with SLC ( $\lambda = 0.1$  meV) and (**e**) without SLC ( $\lambda = 0$  meV). Dashed rectangles in **d, e** mark the first Brillouin zone. White arrows in **c, d** indicate the same avoided crossing. All results are obtained for the model of a 2D honeycomb antiferromagnet with Heisenberg-Kitaev-Gamma-Gamma' interactions ( $J_1 = -3.2$  meV,  $J_2 = 0.1$  meV,  $J_3 = 1.2$  meV,  $K = 2.7$  meV,  $\Gamma = -2.9$  meV, and  $\Gamma' = 1.6$  meV) and coupling of the spins to out-of-plane lattice displacements (see text for further details).

- [1] K. v. Klitzing, G. Dorda, and M. Pepper, *New Method for High-Accuracy Determination of the Fine-Structure Constant Based on Quantized Hall Resistance*, Phys. Rev. Lett. **45**, 494 (1980).
- [2] D. J. Thouless, M. Kohmoto, M. P. Nightingale, and M. den Nijs, *Quantized Hall Conductance in a Two-Dimensional Periodic Potential*, Phys. Rev. Lett. **49**, 405 (1982).
- [3] F. D. M. Haldane, *Model for a Quantum Hall Effect without Landau Levels: Condensed-Matter Realization of the “Parity Anomaly,”* Phys. Rev. Lett. **61**, 2015 (1988).
- [4] P. W. Anderson, *Resonating Valence Bonds: A New Kind of Insulator?*, Materials Research Bulletin **8**, 153 (1973).
- [5] R. Moessner and S. L. Sondhi, *Resonating Valence Bond Phase in the Triangular Lattice Quantum Dimer Model*, Phys. Rev. Lett. **86**, 1881 (2001).
- [6] A. Kitaev, *Anyons in an Exactly Solved Model and Beyond*, Annals of Physics **321**, 2 (2006).
- [7] A. Stern and N. H. Lindner, *Topological Quantum Computation—From Basic Concepts to First Experiments*, Science **339**, 1179 (2013).
- [8] V. Lahtinen and J. Pachos, *A Short Introduction to Topological Quantum Computation*, SciPost Physics **3**, 021 (2017).
- [9] H. Katsura, N. Nagaosa, and P. A. Lee, *Theory of the Thermal Hall Effect in Quantum Magnets*, Phys. Rev. Lett. **104**, 066403 (2010).
- [10] R. Matsumoto, R. Shindou, and S. Murakami, *Thermal Hall Effect of Magnons in Magnets with Dipolar Interaction*, Phys. Rev. B **89**, 054420 (2014).
- [11] J. Nasu, J. Yoshitake, and Y. Motome, *Thermal Transport in the Kitaev Model*, Phys. Rev. Lett. **119**, 127204 (2017).
- [12] Y. Kasahara, T. Ohnishi, Y. Mizukami, O. Tanaka, S. Ma, K. Sugii, N. Kurita, H. Tanaka, J. Nasu, Y. Motome, T. Shibauchi, and Y. Matsuda, *Majorana Quantization and Half-Integer Thermal Quantum Hall Effect in a Kitaev Spin Liquid*, Nature **559**, 7713 (2018).
- [13] J. Romhányi, K. Penc, and R. Ganesh, *Hall Effect of Triplons in a Dimerized Quantum Magnet*, Nat Commun **6**, 1 (2015).
- [14] P. A. McClarty, F. Krüger, T. Guidi, S. F. Parker, K. Refson, A. W. Parker, D. Prabhakaran, and R. Coldea, *Topological Triplon Modes and Bound States in a Shastry–Sutherland Magnet*, Nature Phys **13**, 8 (2017).
- [15] S. Raghu and F. D. M. Haldane, *Analogs of Quantum-Hall-Effect Edge States in Photonic Crystals*, Phys. Rev. A **78**, 033834 (2008).
- [16] L. Lu, J. D. Joannopoulos, and M. Soljačić, *Topological Photonics*, Nature Photon **8**, 11 (2014).
- [17] Y. Onose, T. Ideue, H. Katsura, Y. Shiomi, N. Nagaosa, and Y. Tokura, *Observation of the Magnon Hall Effect*, Science (2010).
- [18] T. Ideue, Y. Onose, H. Katsura, Y. Shiomi, S. Ishiwata, N. Nagaosa, and Y. Tokura, *Effect of Lattice Geometry on Magnon Hall Effect in Ferromagnetic Insulators*, Phys. Rev. B **85**, 134411 (2012).
- [19] R. Shindou, R. Matsumoto, S. Murakami, and J. Ohe, *Topological Chiral Magnonic Edge Mode in a Magnonic Crystal*, Phys. Rev. B **87**, 174427 (2013).
- [20] A. Mook, J. Henk, and I. Mertig, *Magnon Hall Effect and Topology in Kagome Lattices: A Theoretical Investigation*, Phys. Rev. B **89**, 134409 (2014).
- [21] R. Chisnell, J. S. Helton, D. E. Freedman, D. K. Singh, R. I. Bewley, D. G. Nocera, and Y. S. Lee, *Topological Magnon Bands in a Kagome Lattice Ferromagnet*, Phys. Rev. Lett. **115**, 147201 (2015).
- [22] A. Mook, J. Henk, and I. Mertig, *Thermal Hall Effect in Noncollinear Coplanar Insulating Antiferromagnets*, Phys. Rev. B **99**, 014427 (2019).
- [23] R. R. Neumann, A. Mook, J. Henk, and I. Mertig, *Thermal Hall Effect of Magnons in Collinear Antiferromagnetic Insulators: Signatures of Magnetic and Topological Phase*

- Transitions*, Phys. Rev. Lett. **128**, 117201 (2022).
- [24] R. Takahashi and N. Nagaosa, *Berry Curvature in Magnon-Phonon Hybrid Systems*, Phys. Rev. Lett. **117**, 217205 (2016).
- [25] S. Zhang, G. Go, K.-J. Lee, and S. K. Kim, *SU(3) Topology of Magnon-Phonon Hybridization in 2D Antiferromagnets*, Phys. Rev. Lett. **124**, 147204 (2020).
- [26] H. Zhang, C. Xu, C. Carnahan, M. Sretenovic, N. Suri, D. Xiao, and X. Ke, *Anomalous Thermal Hall Effect in an Insulating van Der Waals Magnet*, Phys. Rev. Lett. **127**, 247202 (2021).
- [27] L. Viciu, Q. Huang, E. Morosan, H. W. Zandbergen, N. I. Greenbaum, T. McQueen, and R. J. Cava, *Structure and Basic Magnetic Properties of the Honeycomb Lattice Compounds  $\text{Na}_2\text{Co}_2\text{TeO}_6$  and  $\text{Na}_3\text{Co}_2\text{SbO}_6$* , Journal of Solid State Chemistry **180**, 1060 (2007).
- [28] E. Lefrançois, M. Songvilay, J. Robert, G. Nataf, E. Jordan, L. Chaix, C. V. Colin, P. Lejay, A. Hadj-Azzem, R. Ballou, and V. Simonet, *Magnetic Properties of the Honeycomb Oxide  $\text{Na}_2\text{Co}_2\text{TeO}_6$* , Phys. Rev. B **94**, 214416 (2016).
- [29] A. K. Bera, S. M. Yusuf, A. Kumar, and C. Ritter, *Zigzag Antiferromagnetic Ground State with Anisotropic Correlation Lengths in the Quasi-Two-Dimensional Honeycomb Lattice Compound  $\text{Na}_2\text{Co}_2\text{TeO}_6$* , Phys. Rev. B **95**, 094424 (2017).
- [30] G. Xiao, Z. Xia, W. Zhang, X. Yue, S. Huang, X. Zhang, F. Yang, Y. Song, M. Wei, H. Deng, and D. Jiang, *Crystal Growth and the Magnetic Properties of  $\text{Na}_2\text{Co}_2\text{TeO}_6$  with Quasi-Two-Dimensional Honeycomb Lattice*, Crystal Growth & Design **19**, 2658 (2019).
- [31] W. Yao and Y. Li, *Ferrimagnetism and Anisotropic Phase Tunability by Magnetic Fields in  $\text{Na}_2\text{Co}_2\text{TeO}_6$* , Phys. Rev. B **101**, 085120 (2020).
- [32] M. Songvilay, J. Robert, S. Petit, J. A. Rodriguez-Rivera, W. D. Ratcliff, F. Damay, V. Balédent, M. Jiménez-Ruiz, P. Lejay, E. Pachoud, A. Hadj-Azzem, V. Simonet, and C. Stock, *Kitaev Interactions in the Co Honeycomb Antiferromagnets  $\text{Na}_3\text{Co}_2\text{SbO}_6$  and  $\text{Na}_2\text{Co}_2\text{TeO}_6$* , Phys. Rev. B **102**, 224429 (2020).
- [33] W. Chen, X. Li, Z. Hu, Z. Hu, L. Yue, R. Sutarto, F. He, K. Iida, K. Kamazawa, W. Yu, X. Lin, and Y. Li, *Spin-Orbit Phase Behavior of  $\text{Na}_2\text{Co}_2\text{TeO}_6$  at Low Temperatures*, Phys. Rev. B **103**, L180404 (2021).
- [34] G. Lin, J. Jeong, C. Kim, Y. Wang, Q. Huang, T. Masuda, S. Asai, S. Itoh, G. Günther, M. Russina, et al., *Field-Induced Quantum Spin Disordered State in Spin-1/2 Honeycomb Magnet  $\text{Na}_2\text{Co}_2\text{TeO}_6$* , Nat Commun **12**, 1 (2021).
- [35] C. Kim, J. Jeong, G. Lin, P. Park, T. Masuda, S. Asai, S. Itoh, H.-S. Kim, H. Zhou, J. Ma, and J.-G. Park, *Antiferromagnetic Kitaev Interaction in  $J_{\text{eff}} = 1/2$  Cobalt Honeycomb Materials  $\text{Na}_3\text{Co}_2\text{SbO}_6$  and  $\text{Na}_2\text{Co}_2\text{TeO}_6$* , J. Phys.: Condens. Matter **34**, 045802 (2021).
- [36] A. M. Samarakoon, Q. Chen, H. Zhou, and V. O. Garlea, *Static and Dynamic Magnetic Properties of Honeycomb Lattice Antiferromagnets  $\text{Na}_2\text{M}_2\text{TeO}_6$ ,  $M=\text{Co}$  and  $\text{Ni}$* , Phys. Rev. B **104**, 184415 (2021).
- [37] G. Xiao, Z. Xia, Y. Song, and L. Xiao, *Magnetic Properties and Phase Diagram of Quasi-Two-Dimensional  $\text{Na}_2\text{Co}_2\text{TeO}_6$  Single Crystal under High Magnetic Field*, J. Phys.: Condens. Matter **34**, 075801 (2021).
- [38] A. L. Sanders, R. A. Mole, J. Liu, A. J. Brown, D. Yu, C. D. Ling, and S. Rachel, *Dominant Kitaev Interactions in the Honeycomb Materials  $\text{Na}_3\text{Co}_2\text{SbO}_6$  and  $\text{Na}_2\text{Co}_2\text{TeO}_6$* , Phys. Rev. B **106**, 014413 (2022).
- [39] W. G. F. Krüger, W. Chen, X. Jin, Y. Li, and L. Janssen, *Triple-Q Order in  $\text{Na}_2\text{Co}_2\text{TeO}_6$  from Proximity to Hidden-SU(2)-Symmetric Point*, arXiv:2211.16957.
- [40] W. Yao, Y. Zhao, Y. Qiu, C. Balz, J. R. Stewart, J. W. Lynn, and Y. Li, *Magnetic Ground State of the Kitaev  $\text{Na}_2\text{Co}_2\text{TeO}_6$  Spin Liquid Candidate*, arXiv:2211.16941.
- [41] S. Zhang, S. Lee, A. J. Woods, W. K. Peria, S. M. Thomas, R. Movshovich, E. Brosha, Q. Huang, H. Zhou, V. S. Zapf, and M. Lee, *Electronic and Magnetic Phase Diagrams*

- of the Kitaev Quantum Spin Liquid Candidate  $\text{Na}_2\text{Co}_2\text{TeO}_6$ , *Phys. Rev. B* **108**, 064421 (2023).
- [42] S. Guang, N. Li, Q. Huang, K. Xia, Y. Wang, H. Liang, Y. Sun, Q. Li, X. Zhao, R. L. Luo, G. Chen, H. Zhou, and X. Sun, *Anisotropic In-Plane Heat Transport of Kitaev Magnet  $\text{Na}_2\text{Co}_2\text{TeO}_6$* , arXiv:2307.06316.
- [43] Y. Singh, S. Manni, J. Reuther, T. Berlijn, R. Thomale, W. Ku, S. Trebst, and P. Gegenwart, *Relevance of the Heisenberg-Kitaev Model for the Honeycomb Lattice Iridates  $\text{A}_2\text{IrO}_3$* , *Phys. Rev. Lett.* **108**, 127203 (2012).
- [44] K. W. Plumb, J. P. Clancy, L. J. Sandilands, V. V. Shankar, Y. F. Hu, K. S. Burch, H.-Y. Kee, and Y.-J. Kim,  $\alpha\text{-RuCl}_3$ : A Spin-Orbit Assisted Mott Insulator on a Honeycomb Lattice, *Phys. Rev. B* **90**, 041112 (2014).
- [45] C. Wong, M. Avdeev, and C. D. Ling, *Zig-Zag Magnetic Ordering in Honeycomb-Layered  $\text{Na}_3\text{Co}_2\text{SbO}_6$* , *Journal of Solid State Chemistry* **243**, 18 (2016).
- [46] See Supplemental Material at [URL will be inserted by publisher] for additional experimental results on magnetometry, heat capacity, and longitudinal thermal conductivity measurements as well as theoretical results on critical magnetic fields, thermal Hall conductivity with and without spin-lattice coupling, and spin fluctuations.
- [47] X. Hong, M. Gillig, R. Hentrich, W. Yao, V. Kocsis, A. R. Witte, T. Schreiner, D. Baumann, N. Pérez, A. U. B. Wolter, Y. Li, B. Büchner, and C. Hess, *Strongly Scattered Phonon Heat Transport of the Candidate Kitaev Material  $\text{Na}_2\text{Co}_2\text{TeO}_6$*  *Phys. Rev. B* **104**, 144426 (2021).
- [48] R. Berman, *Thermal Conduction in Solids* (Clarendon Press, 1976).
- [49] S. K. Guang, N. Li, R. L. Luo, Q. Huang, Y. Y. Wang, X. Y. Yue, K. Xia, Q. J. Li, X. Zhao, G. Chen, H. D. Zhou, and X. F. Sun, *Thermal Transport of Fractionalized Antiferromagnetic and Field Induced States in the Kitaev Material  $\text{Na}_2\text{Co}_2\text{TeO}_6$* , arXiv:2211.07914.
- [50] C. Strohm, G. L. J. A. Rikken, and P. Wyder, *Phenomenological Evidence for the Phonon Hall Effect*, *Phys. Rev. Lett.* **95**, 155901 (2005).
- [51] H. Doki, M. Akazawa, H.-Y. Lee, J. H. Han, K. Sugii, M. Shimozawa, N. Kawashima, M. Oda, H. Yoshida, and M. Yamashita, *Spin Thermal Hall Conductivity of a Kagome Antiferromagnet*, *Phys. Rev. Lett.* **121**, 097203 (2018).
- [52] M. Hirschberger, J. W. Krizan, R. J. Cava, and N. P. Ong, *Large Thermal Hall Conductivity of Neutral Spin Excitations in a Frustrated Quantum Magnet*, *Science* **348**, 106 (2015).
- [53] M. Hirschberger, P. Czajka, S. M. Koohpayeh, W. Wang, and N. P. Ong, *Enhanced Thermal Hall Conductivity below 1 Kelvin in the Pyrochlore Magnet  $\text{Yb}_2\text{Ti}_2\text{O}_7$* , arXiv:1903.00595.
- [54] L. Chen, M.-E. Boulanger, Z.-C. Wang, F. Tafti, and L. Taillefer, *Large Phonon Thermal Hall Conductivity in the Antiferromagnetic Insulator  $\text{Cu}_3\text{TeO}_6$* , *Proceedings of the National Academy of Sciences* **119**, e2208016119 (2022).
- [55] M.-E. Boulanger, G. Grissonnanche, É. Lefrançois, A. Gourgout, K.-J. Xu, Z.-X. Shen, R. L. Greene, and L. Taillefer, *Thermal Hall Conductivity of Electron-Doped Cuprates*, *Phys. Rev. B* **105**, 115101 (2022).
- [56] A. Ataei, G. Grissonnanche, M.-E. Boulanger, L. Chen, E. Lefrançois, V. Brouet, and L. Taillefer, *Impurity-Induced Phonon Thermal Hall Effect in the Antiferromagnetic Phase of  $\text{Sr}_2\text{IrO}_4$* , arXiv:2302.03796.
- [57] J. G. Rau, E. K.-H. Lee, and H.-Y. Kee, *Generic Spin Model for the Honeycomb Iridates beyond the Kitaev Limit*, *Phys. Rev. Lett.* **112**, 077204 (2014).
- [58] J. Chaloupka and G. Khaliullin, *Hidden Symmetries of the Extended Kitaev-Heisenberg Model: Implications for the Honeycomb-Lattice Iridates  $\text{A}_2\text{IrO}_3$* , *Phys. Rev. B* **92**, 024413 (2015).



- [59] H. Liu, J. Chaloupka, and G. Khaliullin, *Kitaev Spin Liquid in 3d Transition Metal Compounds*, Phys. Rev. Lett. **125**, 047201 (2020).
- [60] T. Holstein and H. Primakoff, *Field Dependence of the Intrinsic Domain Magnetization of a Ferromagnet*, Phys. Rev. **58**, 1098 (1940).
- [61] J. H. P. Colpa, *Diagonalization of the Quadratic Boson Hamiltonian*, Physica A: Statistical Mechanics and Its Applications **93**, 327 (1978).
- [62] P. A. Maksimov, Z. Zhu, S. R. White, and A. L. Chernyshev, *Anisotropic-Exchange Magnets on a Triangular Lattice: Spin Waves, Accidental Degeneracies, and Dual Spin Liquids*, Phys. Rev. X **9**, 021017 (2019).
- [63] P. A. Maksimov and A. L. Chernyshev, *Rethinking  $\alpha$ -RuCl<sub>3</sub>*, Phys. Rev. Research **2**, 033011 (2020).
- [64] R. Matsumoto and S. Murakami, *Theoretical Prediction of a Rotating Magnon Wave Packet in Ferromagnets*, Phys. Rev. Lett. **106**, 197202 (2011).
- [65] S. Park and B.-J. Yang, *Topological Magnetoelastic Excitations in Noncollinear Antiferromagnets*, Phys. Rev. B **99**, 174435 (2019).
- [66] X. Zhang, Y. Zhang, S. Okamoto, and D. Xiao, *Thermal Hall Effect Induced by Magnon-Phonon Interactions*, Phys. Rev. Lett. **123**, 167202 (2019).
- [67] G. Go, S. K. Kim, and K.-J. Lee, *Topological Magnon-Phonon Hybrid Excitations in Two-Dimensional Ferromagnets with Tunable Chern Numbers*, Phys. Rev. Lett. **123**, 237207 (2019).
- [68] S. Park, N. Nagaosa, and B.-J. Yang, *Thermal Hall Effect, Spin Nernst Effect, and Spin Density Induced by a Thermal Gradient in Collinear Ferrimagnets from Magnon-Phonon Interaction*, Nano Lett. **20**, 2741 (2020).
- [69] B. Sheikhi, M. Kargarian, and A. Langari, *Hybrid Topological Magnon-Phonon Modes in Ferromagnetic Honeycomb and Kagome Lattices*, Phys. Rev. B **104**, 045139 (2021).
- [70] B. Ma and G. A. Fiete, *Antiferromagnetic Insulators with Tunable Magnon-Polaron Chern Numbers Induced by in-Plane Optical Phonons*, Phys. Rev. B **105**, L100402 (2022).
- [71] C. Xu, C. Carnahan, H. Zhang, M. Sretenovic, P. Zhang, D. Xiao, and X. Ke, *Thermal Hall Effect in a van Der Waals Triangular Magnet FeCl<sub>2</sub>*, Phys. Rev. B **107**, L060404 (2023).
- [72] E. Thingstad, A. Kamra, A. Brataas, and A. Sudbø, *Chiral Phonon Transport Induced by Topological Magnons*, Phys. Rev. Lett. **122**, 107201 (2019).
- [73] N. Bazazzadeh, M. Hamdi, S. Park, A. Khavasi, S. M. Mohseni, and A. Sadeghi, *Magnetoelastic Coupling Enabled Tunability of Magnon Spin Current Generation in Two-Dimensional Antiferromagnets*, Phys. Rev. B **104**, L180402 (2021).
- [74] A. Tari, *The Specific Heat of Matter at Low Temperatures* (Imperial College Press, 2003).